Linear semiconductor optical amplifiers for amplification of advanced modulation formats

R. Bonk,[1,*] G. Huber,[1] T. Vallaitis,[1] S. Koenig,[1] R. Schmogrow,[1] D. Hillerkuss,[1] R. Brenot,[2] F. Lelarge,[2] G.-H. Duan,[2] S. Sygletos,[1,3] C. Koos,[1,4] W. Freude,[1,4] and J. Leuthold[1,4]

[1]*Institute of Photonics and Quantum Electronics (IPQ), Karlsruhe Institute of Technology (KIT), Engesserstr. 5, 76131 Karlsruhe, Germany*

[2]*III-V Lab, a joint lab of Alcatel-Lucent Bell Labs France, Thales Research and Technology and CEA Leti, Campus Polytechnique, 1, Avenue A. Fresnel, 91767 Palaiseau cedex, France*

[3]*Photonic Systems Group, Tyndall National Institute, University College Cork, Lee Maltings, Dyke Parade, Cork, Ireland*

[4]*Institute of Microstructure Technology (IMT), Karlsruhe Institute of Technology (KIT), Hermann-von-Helmholtz-Platz 1, 76344 Eggenstein-Leopoldshafen, Germany*

**rene.bonk@kit.edu*

Abstract: The capability of semiconductor optical amplifiers (SOA) to amplify advanced optical modulation format signals is investigated. The input power dynamic range is studied and especially the impact of the SOA alpha factor is addressed. Our results show that the advantage of a lower alpha-factor SOA decreases for higher-order modulation formats. Experiments at 20 GBd BPSK, QPSK and 16QAM with two SOAs with different alpha factors are performed. Simulations for various modulation formats support the experimental findings.

OCIS codes: (250.5980) Semiconductor optical amplifiers; (250.5590) Quantum-well, -wire and -dot devices; (060.1660) Coherent communications.

References and links

1. R. Bonk, T. Vallaitis, J. Guetlein, C. Meuer, H. Schmeckebier, and D. Bimberg. C. Koos, W. Freude, and J. Leuthold, "The input power dynamic range of a semiconductor optical amplifier and its relevance for access network applications," IEEE Photonics J. **3**, 1039–1053 (2011).
2. R. J. Manning, D. A. O. Davies, and J. K. Lucek, "Recovery rates in semiconductor laser amplifiers: optical and electrical bias dependencies," Electron. Lett. **30**, 1233–1235 (1994).
3. D. Wolfson, S. L. Danielsen, C. Joergensen, B. Mikkelsen, and K. E. Stubkjaer, "Detailed theoretical investigation of the input power dynamic range for gain-clamped semiconductor optical amplifier gates at 10 Gb/s," IEEE Photon. Technol. Lett. **10**, 1241–1243 (1998).
4. D. A. Francis, S. P. DiJaili, and J. D. Walker, "A single-chip linear optical amplifier," *in Optical Fiber Communication Conference, OSA Technical Digest Series (Optical Society of America, 2001),* paper PD13.
5. C. Michie, A. E. Kelly, I. Armstrong, I. Andonovic, and C. Tombling, "An adjustable gain-clamped semiconductor optical amplifier (AGC-SOA)," J. Lightwave Technol. **25**, 1466–1473 (2007).
6. H. N. Tan, M. Matsuura, and N. Kishi, "Enhancement of input power dynamic range for multiwavelength amplification and optical signal processing in a semiconductor optical amplifier using holding beam effect," J. Lightwave Technol. **8**, 2593–2602 (2010).
7. J. Yu and P. Jeppesen, "Increasing input power dynamic range of SOA by shifting the transparent wavelength of tunable optical filter," J. Lightwave Technol. **19**, 1316–1325 (2001).
8. J. Leuthold, D. M. Marom, S. Cabot, J. J. Jaques, R. Ryf, and C. R. Giles, "All-optical wavelength conversion using a pulse reformatting optical filter," J. Lightwave Technol. **22**, 186–192 (2004).
9. P. J. Winzer and R.-J. Essiambre, "Advanced modulation formats for high-capacity optical transport networks," J. Lightwave Technol. **24**, 4711–4728 (2006).
10. M. Sauer and J. Hurley, "Experimental 43 Gb/s NRZ and DPSK performance comparison for systems with up to 8 concatenated SOAs," in *Conference on Lasers and Electro-Optics/Quantum Electronics and Laser Science Conference and Photonic Applications Systems Technologies, Technical Digest (CD) (Optical Society of America, 2006),* paper CThY2.
11. E. Ciaramella, A. D'Errico, and V. Donzella, "Using semiconductor-optical amplifiers with constant envelope WDM signals," IEEE J. Quantum Electron. **44**, 403–409 (2008).
12. J. D. Downie and J. Hurley, "Effects of dispersion on SOA nonlinear impairments with DPSK signals," in *Proc. of 21st Annual Meeting of the IEEE Lasers and Electro-Optics Society, LEOS 2008,* paper WX3.

#163313 - $15.00 USD Received 22 Feb 2012; revised 9 Apr 2012; accepted 9 Apr 2012; published 12 Apr 2012

13. P. S. Cho, Y. Achiam, G. Levy-Yurista, M. Margalit, Y. Gross, and J. B. Khurgin, "Investigation of SOA nonlinearities on the amplification of high spectral efficiency signals," *in Optical Fiber Communication Conference, OSA Technical Digest (CD) (Optical Society of America, 2004),* paper MF70.
14. X. Wei, Y. Su, X. Liu, J. Leuthold, and S. Chandrasekhar, "10-Gb/s RZ-DPSK transmitter using a saturated SOA as a power booster and limiting amplifier," IEEE Photon. Technol. Lett. **16**, 1582–1584 (1998).
15. H. Takeda, N. Hashimoto, T. Akashi, H. Narusawa, K. Matsui, K. Mori, S. Tanaka, and K. Morito, "Wide range over 20 dB output power control using semiconductor optical amplifier for 43.1 Gbps RZ-DQPSK signal," *35th European Conference on Optical Communication, 2009. ECOC 2009,* paper 5.3.4, *http://ieeexplore.ieee.org/stamp/stamp.jsp?tp=&arnumber=5287100&isnumber=5286960*.
16. T. Vallaitis, R. Bonk, J. Guetlein, D. Hillerkuss, J. Li, R. Brenot, F. Lelarge, G.-H. Duan, W. Freude, and J. Leuthold, "Quantum dot SOA input power dynamic range improvement for differential-phase encoded signals," Opt. Express **18**(6), 6270–6276 (2010).
17. R. Bonk, G. Huber, T. Vallaitis, R. Schmogrow, D. Hillerkuss, C. Koos, W. Freude, and J. Leuthold, "Impact of alfa-factor on SOA dynamic range for 20 GBd BPSK, QPSK and 16-QAM signals," in *Optical Fiber Communication Conference, OSA Technical Digest (CD) (Optical Society of America, 2011),* paper OML4.
18. N. A. Olsson, "Lightwave systems with optical amplifiers," J. Lightwave Technol. **7**, 1071–1082 (1989), http://ieeexplore.ieee.org/stamp/stamp.jsp?tp=&arnumber=29634&isnumber=1269.
19. C. Meuer, J. Kim, M. Laemmlin, S. Liebich, A. Capua, G. Eisenstein, A. R. Kovsh, S. S. Mikhrin, I. L. Krestnikov, and D. Bimberg, "Static gain saturation in quantum dot semiconductor optical amplifiers," Opt. Express **16**(11), 8269–8279 (2008).
20. G.-W. Lu, M. Sköld, P. Johannisson, J. Zhao, M. Sjödin, H. Sunnerud, M. Westlund, A. Ellis, and P. A. Andrekson, "40-Gbaud 16-QAM transmitter using tandem IQ modulators with binary driving electronic signals," Opt. Express **18**(22), 23062–23069 (2010).
21. T. Vallaitis, C. Koos, R. Bonk, W. Freude, M. Laemmlin, C. Meuer, D. Bimberg, and J. Leuthold, "Slow and fast dynamics of gain and phase in a quantum dot semiconductor optical amplifier," Opt. Express **16**(1), 170–178 (2008).
22. R. Giller, R. J. Manning, and D. Cotter, "Gain and phase recovery of optically excited semiconductor optical amplifiers," IEEE Photon. Technol. Lett. **18**, 1061–1063 (2006).
23. J. Wang, A. Maitra, C. G. Poulton, W. Freude, and J. Leuthold, "Temporal dynamics of the alpha factor in semiconductor optical amplifiers," J. Lightwave Technol. **25**, 891–900 (2007), http://ieeexplore.ieee.org/stamp/stamp.jsp?tp=&arnumber=1621277&isnumber=33924.
24. W. Loh, J. J. Plant, J. Klamkin, J. P. Donnelly, F. J. O'Donnell, R. J. Ram, and P. W. Juodawlkis, "Noise figure of Watt-class ultralow-confinement semiconductor optical amplifiers," IEEE J. Quantum Electron. **47**, 66–75 (2011).
25. A. Borghesani, "Semiconductor optical amplifiers for advanced optical applications," *International Conference on Transparent Optical Networks, ICTON 2006,* 119–122.
26. A. V. Uskov, T. W. Berg, and J. Mørk, "Theory of pulse-train amplification without patterning effects in quantum-dot semiconductor optical amplifiers," IEEE J. Quantum Electron. **40**, 306–320 (2004).
27. A. V. Uskov, E. P. O'Reilly, M. Laemmlin, N. N. Ledentsov, and D. Bimberg, "On gain saturation in quantum dot semiconductor optical amplifiers," Opt. Commun. **248**, 211–219 (2005).
28. S. Sygletos, R. Bonk, T. Vallaitis, A. Marculescu, P. Vorreau, J. S. Li, R. Brenot, F. Lelarge, G. H. Duan, W. Freude, and J. Leuthold, "Filter assisted wavelength conversion with quantum-dot SOAs," J. Lightwave Technol. **28**, 882–897 (2010).
29. A. V. Uskov, J. Mørk, B. Tromberg, T. W. Berg, I. Magnusdottir, and E. P. O'Reilly, "On high-speed cross-gain modulation without pattern effects in quantum dot semiconductor optical amplifiers," Opt. Commun. **227**, 363–369 (2003).
30. A. V. Uskov, E. P. O'Reilly, R. J. Manning, R. P. Webb, D. Cotter, M. Laemmlin, N. N. Ledentsov, and D. Bimberg, "On ultrafast switching based on quantum-dot semiconductor optical amplifiers in nonlinear interferometers," IEEE Photon. Technol. Lett. **16**, 1265–1267 (2004).
31. V. J. Urick, J. X. Qiu, and F. Bucholtz, "Wide-band QAM-over-fiber using phase modulation and interferometric demodulation," IEEE Photon. Technol. Lett. **16**, 2374–2376 (2004).
32. R. Schmogrow, B. Nebendahl, M. Winter, A. Josten, D. Hillerkuss, S. Koenig, J. Meyer, M. Dreschmann, M. Huebner, C. Koos, J. Becker, W. Freude, and J. Leuthold, "Error vector magnitude as a performance measure for advanced modulation formats," IEEE Photon. Technol. Lett. **24**, 61–63 (2012).
33. F. Lelarge, B. Dagens, J. Renaudier, R. Brenot, A. Accard, F. van Dijk, D. Make, O. L. Gouezigou, J.-G. Provost, F. Poingt, J. Landreau, O. Drisse, E. Derouin, B. Rousseau, F. Pommereau, and G.-H. Duan, "Recent advances on InAs/InP quantum dash based semiconductor lasers and optical amplifiers operating at 1.55μm," IEEE J. Sel. Top. Quantum Electron. **13**, 111–124 (2007).
34. C. Dorrer and I. Kang, "Real-time implementation of linear spectrograms for the characterization of high bit-rate optical pulse trains," IEEE Photon. Technol. Lett. **16**, 858–860 (2004).
35. R. Schmogrow, D. Hillerkuss, M. Dreschmann, M. Huebner, M. Winter, J. Meyer, B. Nebendahl, C. Koos, J. Becker, W. Freude, and J. Leuthold, "Real-time software-defined multiformat transmitter generating 64 QAM at 28 GBd," IEEE Photon. Technol. Lett. **22**, 1601–1603 (2010).</jrn>

#163313 - $15.00 USD Received 22 Feb 2012; revised 9 Apr 2012; accepted 9 Apr 2012; published 12 Apr 2012

1. Introduction

Semiconductor optical amplifiers (SOA) will need to cope with advanced modulation format signals in next-generation optical networks. In particular, the complexity of emitters and receivers may require integrated boosters or pre-amplifiers to compensate the losses of the multi-stage modulation and demodulation steps. The question though is how well SOAs can amplify advanced modulation format data signals and which parameters matter in the selection of an SOA. Further, it is of interest how the parameters need to be optimized in the SOA design for an optimum operation with such modulation formats.

An ideal SOA for advanced modulation formats needs to amplify symbols with both small and large amplitudes alike. This presumably requires an SOA with a large input power dynamic range (IPDR). The IPDR defines the power range in which error-free amplification can be achieved [1]. A large IPDR is obtained when the SOA has a large saturation input power $P_{\mathrm{sat}}^{\mathrm{in}}$ such that it can cope with largest amplitudes as well as when the SOA has a low noise figure such that it can deal with weak amplitudes. Successful attempts towards increasing the linear operation range for on-off-keying (OOK) data signals were by introducing gain clamped SOA or holding beam techniques [2–6]. Other approaches exploited special filter arrangements [7,8] in order to mitigate the bit pattern effects of an SOA when operated in its nonlinear regime. However, a recent detailed study for OOK modulation formats revealed that conventional SOAs may as well offer a large IPDR exceeding 40 dB (at a bit error ratio of 10^{-5}) when properly designed [1].

But, an ideal SOA for advanced modulation formats not only needs to properly amplify signals with various amplitude and power levels but also should preserve the phase relations between the symbols [9]. Prior work on SOA has focused on phase-shift keying (PSK) modulation formats such as differential phase-shift keying signals (DPSK) [10–14] and differential quadrature phase-shift keying signals (DQPSK) [15,16]. These modulation formats basically have a constant modulus and therefore naturally may be anticipated to be more tolerant towards SOA nonlinearities.

However, so-called M-ary quadrature amplitude modulation (QAM) formats comprise both amplitude-shift keying (ASK) and PSK aspects. Thus an ideal SOA should amplify such QAM signals with high amplitude and phase fidelity. In SOAs gain changes and phase changes are related by the so-called Henry's alpha factor α_{H}. Thus, one might assume that a low alpha factor SOA is advantageous. As quantum-dot (QD) SOAs tend to have lower alpha factors one might expect that they should outperform bulk SOA as amplifiers for advanced modulation formats. Yet, a recent publication showed that things get more intricate when QAM signals are used [17].

In this paper, we show that SOAs for advanced modulation formats primarily need to be optimized for a large IPDR (i. e. linear operation with low noise figure). Additionally, an SOA with a low alpha factor offers advantages when modulation formats are not too complex. The findings are substantiated by both simulations and experiments performed on SOAs with different alpha factors for various advanced modulation formats. In particular it is shown that the IPDR advantage of a QD SOA with a low alpha factor reduces when changing the modulation format from binary phase-shift-keying BPSK (2QAM) to quadrature phase-shift-keying QPSK (4QAM) and it vanishes completely for 16QAM. This significant change is due to the smaller probability of large power transitions if the number M of constellation points increases. The smaller probability of large power transitions in turn leads to reduced phase errors caused by amplitude-phase coupling via the alpha factor.

The paper is organized as follows: Section 2 covers the effects which limit the signal quality when amplifying signals having advanced modulation formats. Section 3 presents the simulation results for differentially phase encoded, non-differentially phase encoded and QAM signals, respectively. In Section 4 we compare for bulk and QD SOA the measurements of 20 GBd BPSK, QPSK and 16QAM signals. Section 5 states the conclusions of this work.

#163313 - $15.00 USD Received 22 Feb 2012; revised 9 Apr 2012; accepted 9 Apr 2012; published 12 Apr 2012

2. Limits in signal quality when amplifying *M*-ary QAM signals

The quality of signals after an SOA is limited by SOA noise for low input powers [18], and by signal distortions due to gain saturation for large input powers [19]. Saturation of the gain not only induces amplitude errors but also phase errors due to the coupling of the alpha factor. Saturation also may induce inter-channel crosstalk if several wavelength division multiplexing (WDM) channels are simultaneously amplified by the same SOA. The ratio of the lower and upper power limits, inside which the reception is approximately error-free, is expressed by the IPDR. In this paper, the term "error-free" is used for two distinct cases. The first case requires a signal quality which corresponds to a bit error ratio (BER) of 10^{-9}. In the second case, the use of an advanced forward error correction (FEC) is assumed, which allows error-free operation for a raw BER of 10^{-3}.

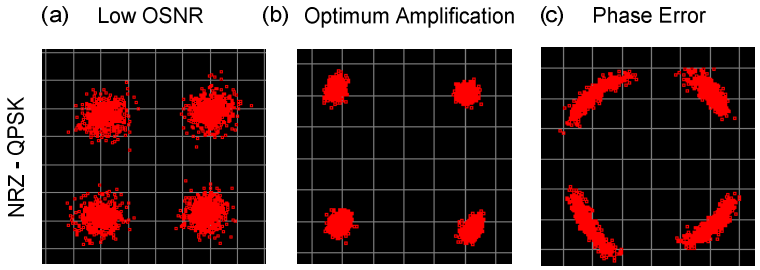

Fig. 1. Constellation diagrams showing the limitations of the signal quality for amplification of a 4QAM (QPSK) data signal. (a) The input power into the SOA is very low resulting in a low OSNR at the output of the amplifier. The constellation diagram of the 4QAM signal shows a symmetrical broadening of the constellation points. This broadening due to ASE noise causes a low signal quality. (b) Error-free amplification of the data signal is observed for a non-saturating input power. (c) For high input powers a nonlinear phase change induced by a refractive index change within the SOA causes a rotation of the constellation points. This rotation causes a reduction of the signal quality.

2.1 Low input power limit

For low input signal powers the limitations are due to amplified spontaneous emission (ASE) noise which in this case is virtually independent of the signal input power. Thus, if the input power decreases while the ASE power remains constant, the optical-signal-to-noise ratio (OSNR) will become poor. An example of such an OSNR limitation is presented in Fig. 1(a) for an optical QPSK (4QAM) signal. The constellation diagram shows a symmetrical broadening of the constellation points. The optimum situation where the input signal power is neither too low nor too high is shown in Fig. 1(b).

2.2 Large input power limit

For large input powers the SOA gain is reduced due to gain saturation. Transitions between symbols are affected by the complex SOA response. Therefore, depending on the modulation format both the amplitude and phase fidelity of the amplification process are impaired to a different degree. Among the many implementations of *M*-PSK and *M*-ary QAM formats the best performing transmitters often use zero-crossing field strength transitions [20], and therefore generate power transitions (solid line), see Fig. 2(a), 2(b). These power transitions change the carrier concentration N and therefore the SOA fiber-to-fiber (FtF) gain $G_{ff} = \exp(g_{ff} L)$, where the FtF net modal gain g_{ff} is assumed to be independent of the SOA length L and comprises the SOA net modal chip gain g ($G = \exp(g L)$) as well as any coupling losses $\alpha_{Coupling}$ to an external fiber, $G_{ff} = \alpha_{Coupling} G \alpha_{Coupling}$, with $1 > \alpha_{Coupling} \geq 0$. A change $\Delta g_{ff} = \Delta(\ln G_{ff}) / L = \Delta g$ of the FtF net modal gain is identical to a change Δg of the net modal gain leading to a change Δn_{eff} of the effective refractive index n_{eff} by amplitude-phase coupling, which in turn is described by the so-called Henry's alpha factor α_H. With the vacuum wave number $k_0 = 2\pi / \lambda_s$, signal wavelength λ_s, the complex output field is in proportion to $(G_{ff})^{0.5}$

#163313 - $15.00 USD Received 22 Feb 2012; revised 9 Apr 2012; accepted 9 Apr 2012; published 12 Apr 2012

$\exp(-\mathrm{j}\, k_0\, n_{\mathrm{eff}}\, L)$ where the output phase (not regarding any input phase modulation) is defined by $\varphi = -k_0\, n_{\mathrm{eff}}\, L$. Output phase change $\Delta\varphi$ and effective refractive index change are related by $\Delta\varphi = -k_0\, \Delta n_{\mathrm{eff}}\, L$. For the alpha factor we then find

$$\alpha_{\mathrm{H}} = \frac{\partial n_{\mathrm{eff}} / \partial N}{\frac{1}{-2k_0}\partial g_{\mathrm{ff}} / \partial N} \approx -2k_0 \frac{\Delta n_{\mathrm{eff}}}{\Delta g_{\mathrm{ff}}} = \frac{2\Delta\varphi}{\Delta g_{\mathrm{ff}}\, L} = \frac{2\Delta\varphi}{\Delta\left(\ln G_{\mathrm{ff}}\right)} = \frac{2\Delta\varphi}{\Delta\left(\ln G\right)}. \qquad (1)$$

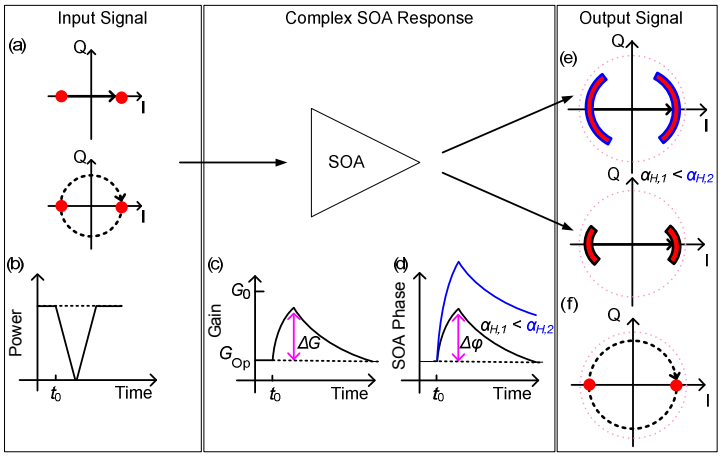

Fig. 2. Response of a saturated SOA in reaction to a BPSK (2QAM) signal with two possible transitions from symbol to symbol. Phase errors induced by power transitions from one BPSK constellation point to the other. (a) BPSK constellation diagram with in-phase (I) and quadrature component (Q) of the electric field. Solid line: zero-crossing transition; dashed line: constant-envelope transition. (b) Time dependencies for the two types of power transitions. SOA response that affects the (c) gain and (d) refractive index which leads to an SOA-induced phase deviation $\Delta\varphi$. SOAs with lower alpha factors induce less amplitude-to-phase conversion and therefore amplify the electric input field with a better phase fidelity. BPSK constellation diagram after amplification with a saturated SOA for (e) zero-crossing transition (for two alpha factors) and (f) constant-envelope transition.

Thus, by amplitude-phase coupling in the SOA, gain changes induce unwanted phase deviations. An illustration of this effect is schematically depicted in Fig. 2 assuming a BPSK format and a saturated SOA. If the signal power reduces at time t_0, Fig. 2(b), the gain starts recovering from its operating point described by a saturated chip gain G_{Op} (given by the average input power) towards the unsaturated small-signal chip gain G_0. After traversing the constellation zero the signal power increases and reduces the gain towards its saturated value G_{Op}, Fig. 2(c). Coupled by the alpha factor, a gain change induces a refractive index change and therefore an SOA-induced phase shift $\Delta\varphi$. SOAs with a lower alpha factor ($\alpha_{\mathrm{H},1} < \alpha_{\mathrm{H},2}$) have less amplitude-to-phase conversion and therefore give rise to less phase changes, see Fig. 2(d), and also Fig. 1(c). As a consequence, SOAs with lower alpha factors are expected to show better signal qualities for phase encoded data with a high probability of large power transitions. The constellation diagrams with induced phase errors are presented in Fig. 2(e) for the two alpha factors. If the transition between the two constellation points maintains a constant envelope (Fig. 2(a), 2(b), dashed line) so that gain and phase changes do not happen (Fig. 2(c), 2(d)), no phase errors occur, Fig. 2(f). If the device could be operated in the small-signal gain region even for high SOA input power levels, the constellation points would lie on the dotted circle. However, due to the described operation under gain saturation, the amplitudes at the SOA output are reduced, see Fig. 2(e), 2(f).

Typically, the phase recovery in SOAs is slower than the gain recovery [21–23], so a phase change induced at the power transition time has not necessarily died out at the time of signal decision (usually in the center of symbol time slot), so that the data phase is perturbed and errors occur. Additionally, the strength of the phase change induced by the SOA and detected at the decision point depends on the required time to change between constellation

#163313 - $15.00 USD Received 22 Feb 2012; revised 9 Apr 2012; accepted 9 Apr 2012; published 12 Apr 2012

points, and thus on the symbol rate and the transmitter bandwidth. If the time to change between constellation points (approximately 10 ps…30 ps for 30 GBd…10 GBd) is not significantly faster than the SOA phase recovery time (about 100 ps), severe phase changes will degrade the signal quality. Thus, only at very high symbol rates, no significant phase change from the SOA is expected indicating the benefit of a limited SOA recovery time. In addition to phase errors amplitude errors are expected to occur in *M-ary* QAM signals. Because *M*-ary QAM signals comprise multiple symbols with different amplitude levels extreme transitions from one corner to the other are less likely. Thus, phase errors due to amplitude-phase coupling are less likely as well. In average the amplitude distances between symbols reduce due to gain saturation.

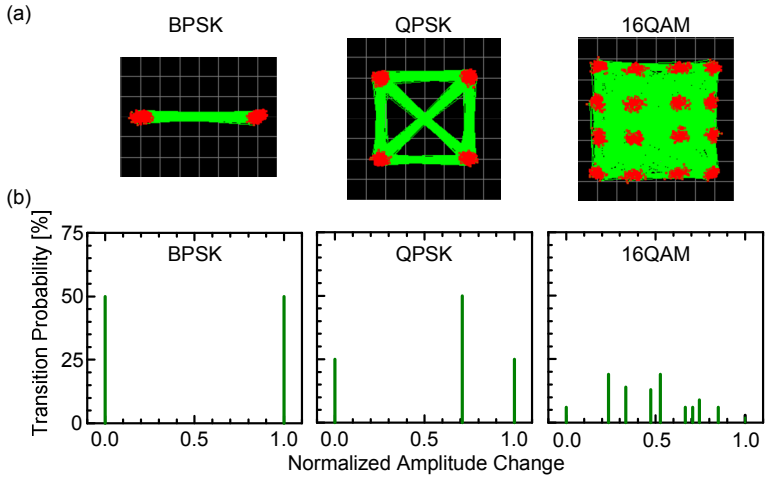

Fig. 3. Constellation diagrams and transition probabilities for different modulation formats. (a) Constellation diagrams with amplitude and phase transitions for BPSK, QPSK and 16QAM data signals. (b) Transition probability as a function of the amplitude change normalized to the largest possible amplitude transition. The probability of large transitions decreases for higher order modulation formats.

Some examples of amplitude transitions in constellation diagrams for practical PSK and *M*-ary QAM implementations are shown in Fig. 3(a) for BPSK, QPSK and 16QAM. The transition probabilities for all occurring normalized amplitude changes are depicted in Fig. 3(b). The transition probability of the largest amplitude change reduces from 50% for BPSK to 25% at QPSK down to below 5% for 16QAM. Thus, the probability to observe a large amplitude change decreases the higher the order of the modulation format.

2.3 Parameters relevant for linear SOAs

In this section, we discuss the parameters which determine the usable input power range of an SOA, namely noise which sets the lower level P_1, and amplifier saturation which is responsible for the upper level P_2. The ratio P_2 / P_1 defines the IPDR for linear operation, a quantity which will be discussed in Section 3.2 in more detail.

The *low input power limit* is basically determined by the ASE noise. The amount of ASE noise added by the SOA is described by the noise figure NF [18], which is defined with the inversion factor n_{sp} and the single-pass chip gain G

$$\mathrm{NF} = \frac{1}{G} + 2n_{sp}\frac{G-1}{G}. \qquad (2)$$

The low input power limit when amplifying data signals with an SOA can be decreased with a lower noise figure. NF is minimized using a population inversion factor n_{sp} approaching 1. This can be achieved by adapting the current density J, i. e. choosing it as high as possible,

#163313 - $15.00 USD Received 22 Feb 2012; revised 9 Apr 2012; accepted 9 Apr 2012; published 12 Apr 2012

with low internal waveguide losses α_{int}, by choosing the proper dimensionality of the electronic system in the active region, i.e. quantum well rather than bulk, and an optimized device structure (e. g. good results have been shown in [24]). A low FtF noise figure NF_{ff} additionally requires a low fiber-to-chip coupling loss at the input.

The *high input power limit* basically is determined by gain saturation induced phase and amplitude changes on the data signal. Thus, a large saturation input power P_{sat}^{in} is required to avoid gain saturation. The saturation input power P_{sat}^{in} can be approximated by

$$P_{sat}^{in} = \left(\frac{hf_s}{G_0 - 2} \frac{2\ln(2)}{\Gamma} \frac{A}{a} \frac{1}{\tau_c} \right), \tag{3}$$

with the Planck constant h, the optical signal carrier frequency f_s, the small-signal chip gain G_0, the area of the active region A, the optical confinement factor Γ, the differential gain a and the effective carrier lifetime τ_c. The high input power limit when amplifying data signals with an SOA can be increased by choosing the gain moderately high, by having a large modal cross section A / Γ, with a doping of the active region to decrease the effective carrier lifetime, with a high bias current density J, and with a low differential gain a. Additionally, if gain saturation cannot be avoided, an SOA with a low alpha-factor and moderately fast gain and phase dynamics are desirable. More details on linear SOA can be found in [1,25].

3. Modeling the impact of the alpha factor on the signal quality

In this section, the impact of the SOA's alpha factor on the amplification of advanced optical modulation format signals is investigated with simulations. Two SOAs with identical performance in terms of unsaturated gain, saturation input power, noise figure, and SOA dynamics are used. The SOAs only differ in their alpha factor. Simulations with alpha factors of 2 and 4 are performed for differentially phase encoded and non-differentially phase encoded data signals, respectively.

3.1 Models for transmitter, SOA and receiver

The simulation environment as shown in Fig. 4 consists of a 28 GBd transmitter (Tx), two virtual switches for either investigating the back-to-back (BtB) signal quality, or for simulating the influence of the SOA on the signal quality. The SOA model takes into account phase changes and ASE noise. The 28 GBd receiver (Rx) is either a direct receiver, a homodyne coherent or a differential (self-coherent) receiver, respectively. In the following each section of the simulation setup is discussed in more detail.

The transmitter (Tx) in Fig. 4 consists of a continuous wave (cw) laser and an optical IQ-modulator. To achieve a realistic signal quality, the electrical signal-to-noise-ratio (SNR) of the modulator input signal in the electrical domain is adjusted to 20 dB. A pulse carver is added in front of the IQ-modulator that either shapes the cw laser light to 33% or 50% RZ pulses, or just lets the cw light pass through for NRZ operation. The electrical data signals supplied to the optical modulator are low-pass filtered with a 3 dB bandwidth of 25 GHz. Jitter of 500 fs and rise and fall times of 8 ps are modeled to mimic realistic optical BtB data signals. This transmitter is used to generate signals with higher-order optical modulation formats such as (D)QPSK and 16QAM. For OOK and (D)BPSK data signals only the I-channel of the IQ-modulator is used. The output signal of the modulator is amplified and subsequently filtered by an optical band pass filter. The in-fiber input power P^{in} to the SOA can be adjusted with an attenuator.

#163313 - $15.00 USD Received 22 Feb 2012; revised 9 Apr 2012; accepted 9 Apr 2012; published 12 Apr 2012

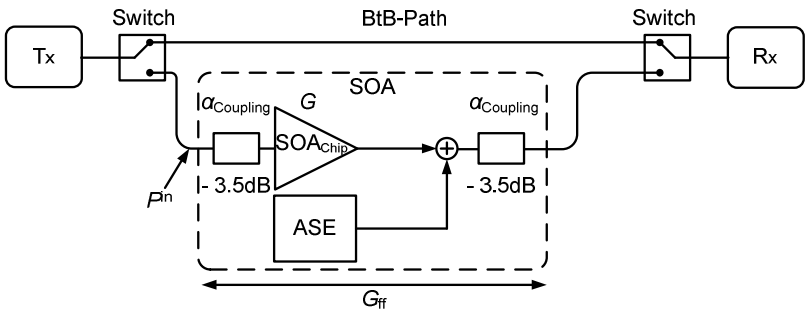

Fig. 4. Simulation environment for investigating the impact of the SOA alpha factor on signals with advanced optical modulation formats. The transmitter (Tx) generates OOK, (D)BPSK, (D)QPSK, or 16QAM data signals. Virtual switches define a reference path for back-to-back (BtB) simulations. The rate-equation based SOA model inside the dashed box provides a chip gain G and takes into account fiber-to-chip losses $\alpha_{Coupling}$ of −3.5 dB per facet, gain-independent amplified spontaneous emission (ASE) noise, and phase changes. Depending of the transmitted data format, the receiver (Rx) is chosen.

The SOA is modeled following the approach in [26–30]. The model describes a quantum-dot (QD) SOA which is longitudinally subdivided into 20 segments. In each segment the evolution of the photon and carrier density along the propagation direction is governed by rate-equations for the photon number and the optical phase. The ASE noise is simulated as white Gaussian noise added to the output of the SOA.

Table 1. Parameter values of the SOA model [26] used in the simulations.

Parameter	Parameter and Value
Current density	$J = 7.5$ kA/cm^2
Area density of QD	$N = 8.5 \times 10^{14}$ m^{-2}
Number of QD layers (separated by spacers and wetting layers (WL))	$l = 6$
Amplifier length	$L = 1$ mm
Thickness of active region	$t_{wg} = 0.125$ µm
Width of active region	$w = 1.75$ µm
Carrier lifetime (WL refilling time)	$\tau_c = 100$ ps
Characteristic relaxation time (QD refilling time)	$\tau_{rel} = 1.25$ ps
Relative line broadening (inhomogeneous/homogeneous)	$\gamma_{inhom} / \gamma_{hom} = 0.33$
Resonant cross section (measure of photon-QD carrier interaction, describing the probability of stimulated radiative transitions)	$\sigma_{res} = 1.3 \times 10^{-19}$ m^2
Internal waveguide losses	$\alpha_{int} = 400$ m^{-1}
Alpha-factor (Henry factor)	$\alpha_H = 2$ and $\alpha_H = 4$
Area density of WL states (WL states serve as a carrier reservoir for QD states)	$n_{wl} = 1.08 \times 10^{16}$ m^{-2}
Average binding energy (energy of QD electrons and holes relative to the WL bandedge)	$\bar{E}_{bind} = 150$ meV

The SOA model parameters are shown in Table 1. The SOA model has been described in [28]. The parameters are chosen to provide a FtF gain G_{ff} of 13.5 dB, a 3 dB in-fiber saturation input power $P_{sat,f}^{in}$ of –2 dBm and a FtF noise figure NF_{ff} of 8.5 dB. The estimated per-facet coupling loss $\alpha_{Coupling}$ is –3.5 dB. To investigate the influence of the alpha factor on the amplification of signals with advanced modulation formats, we simulate two SOAs with alpha factors 2 and 4, respectively. The FtF gain G_{ff} and the FtF noise figure NF_{ff} versus the in-fiber input power P^{in} of the two SOAs are shown in Fig. 5(a) and 5(b). The input signal is set to a wavelength of $\lambda_1 = 1554$ nm. The modulus $|\Delta\varphi|$ of the phase changes of the SOAs are plotted in Fig. 5(c). Large input powers cause carrier depletion. Thus the gain is suppressed, and the phase change due the amplifier saturation increases with increasing input power. The device with the larger alpha factor shows stronger phase changes under gain suppression.

#163313 - $15.00 USD Received 22 Feb 2012; revised 9 Apr 2012; accepted 9 Apr 2012; published 12 Apr 2012

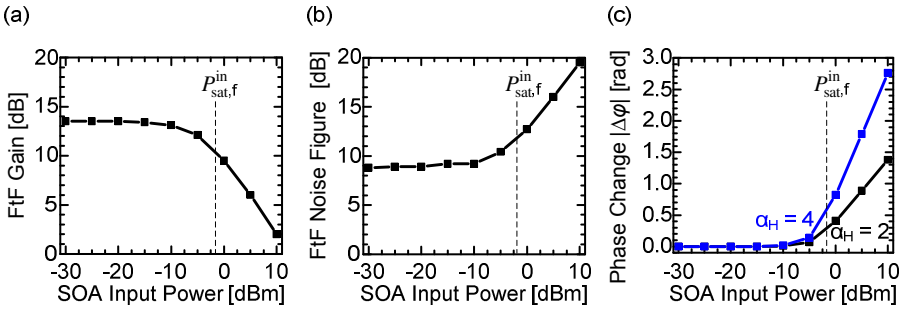

Fig. 5. Comparison of SOA characteristics for devices which only differ in the alpha factor. An SOA with an alpha factor of 2 (black) and an SOA with an alpha factor of 4 (blue) are used for the simulation. (a) FtF gain G_{ff} as a function of the SOA input power is shown. The unsaturated FtF gain G_{f0} is 13.5 dB at a wavelength of 1554 nm, and the 3 dB saturation input power is −2 dBm. (b) FtF noise figure as a function of SOA input power. (c) Phase change $\Delta\varphi \le 0$ as a function of SOA input power. The SOA with larger alpha factor causes larger magnitudes $|\Delta\varphi|$ if the SOA becomes saturated.

The receiver model depends on the modulation format. Basically, it comprises a noisy optical amplifier and a noise-free photoreceiver. Three receiver types are available: For direct detection, for coherent detection and for differential (self-coherent) detection. OOK-formatted (intensity encoded) signals are directly detected with a photodiode. The differentially phase encoded DPSK and DQPSK formats are received with delay interferometer (DI) based demodulators followed by balanced detectors. Signals with non-differentially phase encoded formats such as BPSK, QPSK and 16QAM are received using a homodyne coherent receiver comprising a noise-free local oscillator (LO), and balanced detectors for the in-phase and the quadrature-phase components, respectively.

3.2 Signal quality evaluation by error vector magnitude, Q^2 factor and *IPDR*

To estimate the signal quality of simulated (and measured) data signals after amplification with the SOAs, we employ the error vector magnitude (EVM) for non-differentially phase encoded data signals, and the Q^2 factor method for differentially phase encoded data signals. With these data, we estimate the IPDR of the SOAs.

Advanced modulation formats such as *M*-ary QAM encode the data in amplitude and phase of the optical electric field. The resulting complex amplitude of this field is described by points in a complex IQ constellation plane defined by the real part (in-phase, I) and imaginary part of the electric field (quadrature-phase, Q). Figure 6(a) depicts a transmitted reference constellation point $E_{t,i}$ (●) and the actually received and measured signal vector $E_{r,i}$ (×), which deviates by an error vector $E_{err,i}$ from the reference. We use non data-aided reception and define the EVM for non-differentially phase encoded data signals as the ratio of the root-mean-square (RMS) of the error vector magnitude for a number of I received random symbols, and the largest magnitude of the field strength $E_{t,m}$ belonging to the outermost constellation point,

$$\mathrm{EVM_m} = \frac{\sigma_{\mathrm{err}}}{\left|E_{\mathrm{t,m}}\right|},\ \sigma^2_{\mathrm{err}} = \frac{1}{I}\sum_{i=1}^{I}\left|E_{\mathrm{err},i}\right|^2,\ E_{\mathrm{err,i}} = E_{\mathrm{r},i} - E_{\mathrm{t},i}\ . \tag{4}$$

The errors in magnitude and phase for the received constellation points are also evaluated separately. The EVM measures the quality of an advanced modulation format signal much the same way as it is customary with the Q^2 factor [31,32].

With the measured EVM as in Fig. 6(b), the IPDR is defined as the range of input powers P^{in} into an SOA at which error-free amplification of a data signal can be ensured. The input power limits for error-free amplification are set by the EVM limit $\mathrm{EVM_{lim}}$ corresponding to a

#163313 - $15.00 USD Received 22 Feb 2012; revised 9 Apr 2012; accepted 9 Apr 2012; published 12 Apr 2012

BER of 10^{-9} or 10^{-3}. The ratio of the corresponding powers P_2 and P_1 in Fig. 6(b) define the IPDR measured in dB,

$$\mathrm{IPDR} = 10\log\left(P_2/P_1\right). \tag{5}$$

Our EVM limits are 23.4% for BPSK, 16.4% for QPSK (indicating a BER = 10^{-9}), and 10.6% for 16QAM (indicating a BER = 10^{-3}) [32].

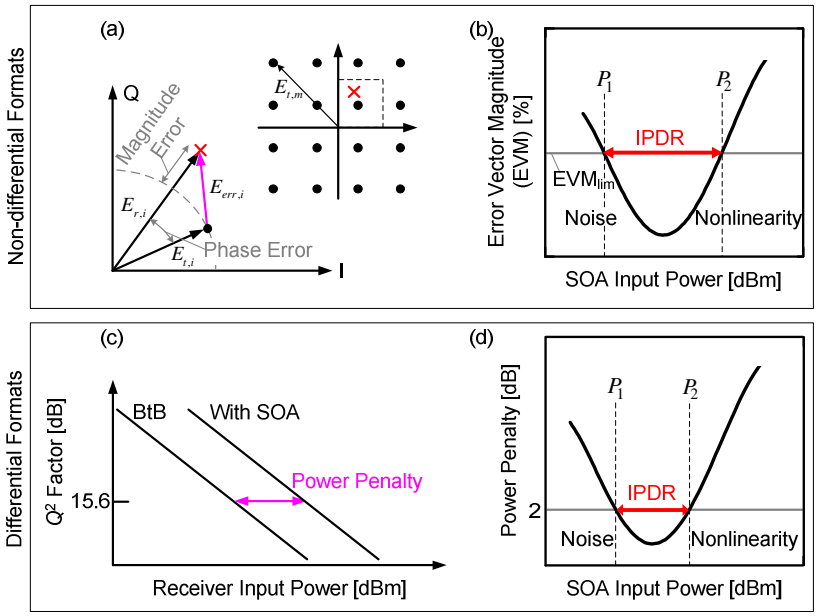

Fig. 6. Error-vector magnitude (EVM), power penalty (PP) and input power dynamic range (IPDR) for non-differential (QAM) and differential (DPSK, DQPSK) modulation formats. For QAM, subfigures (a) and (b) illustrate the EVM definition and the determination of the IPDR for given EVM_{lim}. For DPSK and DQPSK, subfigures (c) and (d) clarify what is meant with the power penalty for a given Q^2 of 15.6 dB, and how the IPDR is determined from a PP of 2 dB.

Differential modulation formats such as DPSK or DQPSK encode information as phase difference between two neighboring bits. On reception, these phase differences are converted into an intensity change by using a delay interferometer demodulator. The signal quality of the obtained eye diagram is estimated by the Q^2 factor irrespective of the fact that demodulated phase noise is not necessarily Gaussian, and that therefore the inferred BER is inaccurate. The I and Q data of the DQPSK signals are evaluated separately and lead to virtually identical Q^2 factors. In Fig. 6(c) the Q^2 factor as a function of receiver input power is presented schematically for the back-to-back case (BtB, without SOA) and for the case with SOA. The power penalty (PP) is the factor by which the power at the receiver input must be increased to compensate for signal degradations compared to the BtB case. In Fig. 6(d) the IPDR for DPSK and DQPSK is again defined according to Eq. (5), but this time by the logarithm of the ratio of SOA input powers P_2 / P_1 for which the PP is less than 2 dB at a Q^2 of 15.6 dB.

3.3 Modulation formats that are advantageous together with low alpha-factor SOAs

In this section, we show by simulation that the use of a low alpha-factor SOA can have an advantage. The alpha factor mostly matters for simple phase encoded signals. Figure 7 shows for both SOA with alpha factors of 2 and 4 the respective EVM and the power penalties as a function of the SOA input powers for (a) BPSK, (b) QPSK, (c) 16QAM, (d) OOK, (e) DPSK and (f) DQPSK. In the case of the DQPSK modulation we considered two variants: The standard NRZ modulation technique which directly switches between different constellation

#163313 - $15.00 USD Received 22 Feb 2012; revised 9 Apr 2012; accepted 9 Apr 2012; published 12 Apr 2012

points so that power transients occur, and a modulation format which maintains a constant signal envelope (red curve in Fig. 7(f) for $\alpha_H = 2$ and $\alpha_H = 4$), so that power transients are absent. The limiting EVM and the limiting power penalty are indicated by gray horizontal lines. The intersections of the EVM or PP curves with these horizontals define the limiting points for the IPDR.

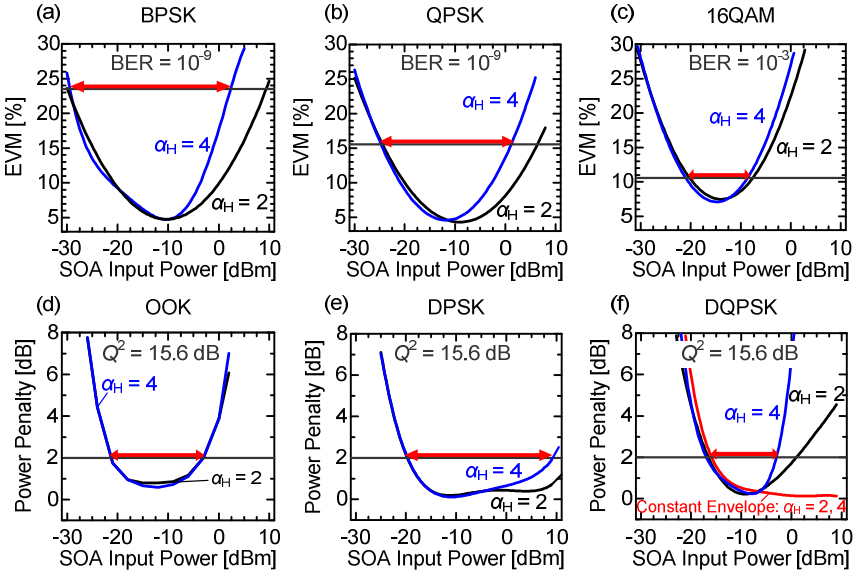

Fig. 7. Simulations illustrate an IPDR advantage for SOA with $\alpha_H = 2$ over SOA with $\alpha_H = 4$, if signals with advanced modulation format and large power transitions between the constellation points are amplified. (a)-(c) EVM as a function of SOA input power for BPSK, QPSK and 16QAM signals (d)-(f) Power penalty as a function of SOA input power for OOK, DPSK and DQPSK signals. The red curve in subfigure (f) assumes a constant-envelope modulation and holds for both, $\alpha_H = 2$ and $\alpha_H = 4$. The IPDR is indicated by red arrows, and the corresponding EVM_{lim} and PP of 2 dB are shown by the gray horizontal lines.

The simulated IPDR for modulation techniques having power transitions between the constellation points reduces from BPSK (2QAM) to QPSK (4QAM) to 16QAM, and from DPSK to DQPSK. The IPDR difference for the SOAs with different alpha factors is largest for the BPSK and the DPSK modulation format, which have the highest probability of large power transition. The power penalty as a function of SOA input power for OOK signal shows, as expected, no difference for the two SOA samples, Fig. 7(d). The results for constant-envelope DQPSK modulation exhibit a very low power penalty at high input powers, Fig. 7(f). This clearly demonstrates the strong influence of power transitions.

Table 2 summarizes the IPDR simulation results for both SOA types. The IPDR values are obtained assuming a certain bit error ratio limit (gray horizontal lines in Fig. 7), and for a specific evaluation method, i. e. PP or EVM. Further, the difference $IPDR_2 - IPDR_4$ of the $IPDR_\alpha$ for the devices with $\alpha_H = 2$ and with $\alpha_H = 4$ is specified.

These results show that:

- For amplifying phase encoded signals, low alpha-factor SOAs are preferable, see $IPDR_2 - IPDR_4$ in Table 2, e. g. rows “NRZ BPSK” and “QPSK”.
- The influence of the alpha factor on high-order *M*-ary QAM signals reduces significantly, compare $IPDR_2 - IPDR_4$ values in Table 2 rows “NRZ BPSK”, “QPSK” with “NRZ 16QAM”.
- As a general tendency the IPDR reduces for increasing complexity of the optical modulation format: For a given average transmitter power the distance between

#163313 - $15.00 USD Received 22 Feb 2012; revised 9 Apr 2012; accepted 9 Apr 2012; published 12 Apr 2012

constellation points reduces with their number, and the required OSNR increases. This moves intersection point P_1 in Fig. 6 to higher powers. On the other hand, if the average power is increased to improve the OSNR, there is a larger risk of amplifier saturation, so that high-power constellation points move closer together. This would shift the intersection point P_2 in Fig. 6 to lower powers.

- Long "1"-sequences of NRZ signals lead to a stronger carrier depletion than "1"-sequences of RZ signals, if the carrier recovery time (100 ps) is in the order of the pulse repetition rate (36 ps). This is the reason why in our case 50% RZ DQPSK modulation leads to an IPDR which is about 14 dB larger than that for NRZ DQPSK, Table 2.

Table 2. Devices with lower alpha factor show larger IPDR for modulation formats with high probability of large power transitions. IPDR for various modulation formats for a symbol rate of 28 GBd for two SOA devices only differing in the alpha factor are shown. The evaluation method, i. e., PP or EVM and the corresponding BER limit are defined. The results of the IPDR difference are also presented. The advantage of a low alpha-factor device manifests in a large IPDR difference.

Format	$-\log_{10}$ BER	$IPDR_\alpha$ [dB]		IPDR Difference
	(PP, EVM)	$\alpha_H = 2$	$\alpha_H = 4$	$IPDR_2 - IPDR_4$ [dB]
33% RZ OOK	9 (PP)	19	19	0
NRZ DPSK	9 (PP)	~ 40	29	~11
NRZ DQPSK	9 (PP)	18	14	4
50% RZ DQPSK	9 (PP)	32	27	5
Const. Envelope DQPSK	9 (PP)	> 30	> 30	$IPDR_{2,4}$ indistinguishable
NRZ BPSK (2QAM)	9 (EVM)	39	32	7
NRZ QPSK (4QAM)	9 (EVM)	31	26	5
NRZ 16QAM	3 (EVM)	14	13	1

4. Measurement results for 20 GBd BPSK, QPSK, and 16QAM signals

To verify the prediction from the simulations two SOA devices are tested with 20 GBd BPSK, QPSK and 16QAM signals. Both SOA are very similar in terms of gain, noise figure, saturation input power as well as dynamics. However, the devices differ in their alpha factors since actually different structures are used, i. e. a bulk and a QD SOA. Here, we focus on the measurement of SOAs amplifying non-differentially phase encoded data signals. In our previous experimental work, results for the differently phase encoded data signals were already presented [16]. All experiments have been performed with 20 GBd rather than 28 GBd due to limitations in our equipment.

4.1. QD and bulk SOA characteristics

For the study we selected devices with similar characteristics. We performed the experiments with a 1.55 µm QD SOA (1 mm length with 6 layers of InAs/InP quantum dots) and a 1.55 µm low optical confinement (20%) bulk SOA (0.7 mm length) [33]. Both were operated at the same current density. Figure 8(a) shows that FtF gain, FtF noise figure and in-fiber saturation input powers are indeed comparable. The gain peak of both devices is around 1530 nm, and the –3 dB bandwidth is 60 nm each. The phase change was measured with a frequency resolved electro-absorption gating (FREAG) technique based on linear spectrograms [34] by evaluating the cross-phase modulation seen on a weak (−15 dBm) cw probe signal in response to a 42.7 Gbit/s '1010…' sequence. The '1'-impulses are 8 ps wide and repeat at a period of 47 ps (duty cycle 17%). For this case, an average input power of + 7 dBm corresponds to a peak input power + 15 dBm. Figure 8(b) shows the phase response of the QD and bulk SOA. The bulk SOA shows 1.7 times higher phase changes than the QD SOA. Therefore, the ratio

#163313 - $15.00 USD Received 22 Feb 2012; revised 9 Apr 2012; accepted 9 Apr 2012; published 12 Apr 2012

of the alpha factors is $\alpha_{H,bulk}$ / $\alpha_{H,QD}$ = 1.7. In Fig. 8(c) the signal quality (Q^2) of a 42.7 Gbit/s RZ OOK data signal with varying SOA input power is shown after amplification with the QD and bulk SOA. The IPDR for the target Q^2 factor of 15.6 dB is around 22 dB for both amplifiers. From these findings we conclude that the devices are comparable with respect to their gain recovery times, and that the overall performance only differs in their phase changes. This fact enables a comparison for advanced modulation format signals in terms of the alpha factor only.

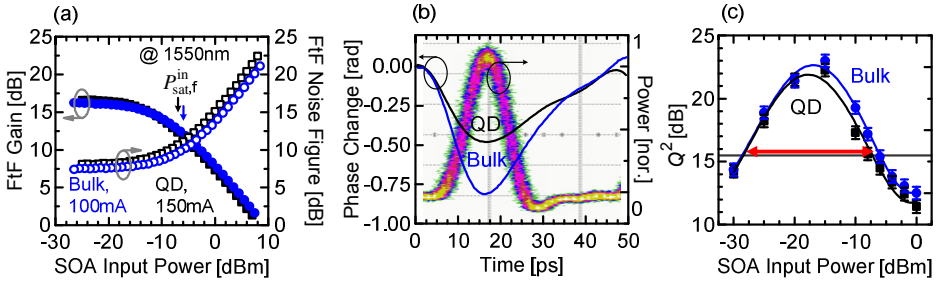

Fig. 8. Comparison of QD and bulk SOA characteristics. (a) FtF gain, FtF noise figure and in-fiber saturation input powers for a 1.55 µm QD SOA (black) and bulk SOA (blue). For equal current densities all characteristics are comparable. (b) Phase response (left vertical axis) in relation to an 8 ps wide impulse (right vertical axis). The bulk SOA shows 1.7 times the peak-to-peak phase change of the QD SOA. (c) Q^2 factor for amplification of a 43 Gbit/s RZ OOK data signal for different device input powers. Since the dynamic range (IPDR indicated by red arrow, gray horizontal line is Q^2 = 15.6 dB) of both SOA is almost identical, the device performance differs only in the alpha factor.

4.2 Multi-format transmitter and coherent receiver

The IPDR for amplification of NRZ BPSK, NRZ QPSK and NRZ 16QAM data signals has been studied by evaluating the EVM [32]. The experimental setup (Fig. 9) comprises a software-defined multi-format transmitter [35] encoding the data onto the optical carrier at 1550 nm, the SOA and a coherent receiver (Agilent N4391A Optical Modulation Analyzer (OMA)). The symbol rate is 20 GBd resulting in 20 Gbit/s BPSK, 40 Gbit/s QPSK and 80 Gbit/s 16QAM signals. The power of the signal is adjusted before launching it into the SOA. After amplification, we analyze EVM as well as magnitude and phase errors. The OMA receives, post-processes, and analyzes the constellations.

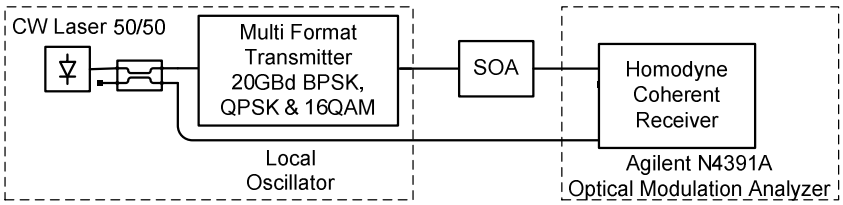

Fig. 9. Experimental setup, comprising a software-defined multi-format transmitter encoding 20 GBd BPSK, QPSK and 16 QAM signals onto an optical carrier. The signal power level is adjusted before launching it to the QD or bulk SOA. The optical modulation analyzer receives, post-processes, and analyzes the data.

4.3 Large IPDR with low alpha-factor SOAs for low-order QAM formats

In Fig. 10(a)-10(c) the EVM for the different modulation formats is depicted as a function of the SOA input power. Figure 10(a) shows for BPSK modulation an IPDR exceeding 36 dB with around 8 dB enhancement for the QD SOA compared to the bulk SOA. Figure 10(b) shows for QPSK modulation an IPDR of 29 dB with an improvement of 4 dB for the QD SOA. The IPDR for 16QAM is 13 dB, and shows no difference between both amplifier types, Fig. 10(c).

#163313 - $15.00 USD Received 22 Feb 2012; revised 9 Apr 2012; accepted 9 Apr 2012; published 12 Apr 2012

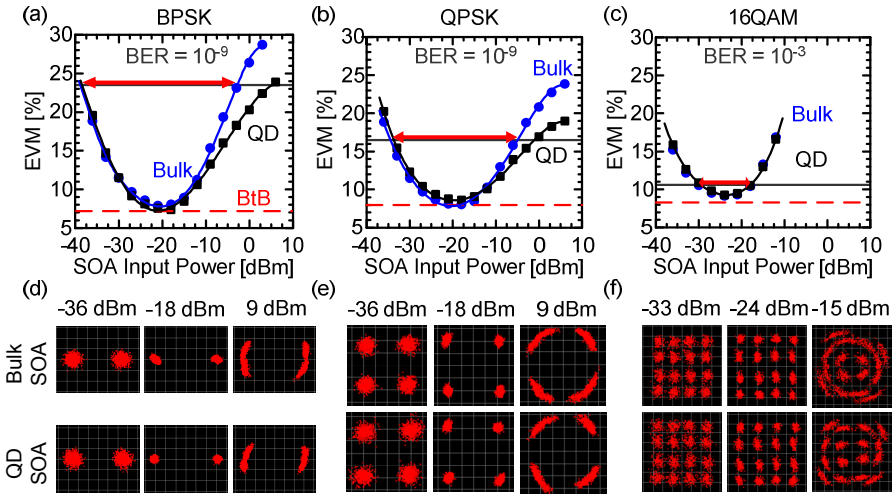

Fig. 10. EVM for different modulation formats and two types of SOA versus input power. (a) Low alpha-factor QD SOA shows an IPDR enhancement of 8 dB compared to bulk SOA for BPSK modulation. In both cases the IPDR exceeds 36 dB. (b) IPDR enhancement at QPSK is reduced, but still 4 dB. An IPDR of 29 dB is found. (c) No difference is found at 16QAM. The IPDR for both devices is 13 dB. The BtB EVMs are indicated by the red dashed lines. The IPDRs are shown by the red arrows, and the gray horizontal lines represent the EVM_{lim}. (d)-(f) Constellation diagrams for various SOA input powers which are associated with the respective subfigure (a)-(c) immediately above. Bulk SOA (upper row) and QD SOA (lower row) are compared.

In addition, in Fig. 10(d)-10(f) constellation diagrams for bulk SOA and QD SOA are presented below the respective EVM subfigures for the three modulation formats, and for three different input power levels. For low input powers the constellations points are broadened by ASE noise. For optimum input powers the constellation points have almost BtB quality. For large input powers the signal quality again reduces. Obviously, the limitation for BPSK and QPSK stems from phase errors, whereas the limitation for the 16QAM signal stems from both, amplitude and phase errors. The phase errors with the PSK formats are larger for the bulk SOA than for the QD SOA.

It has already been shown that EVM is an appropriate metric to estimate the BER and describe the signal quality of an optical channel limited by additive white Gaussian noise [32]. Here, the EVM is also used to estimate the BER if the signal quality is limited by nonlinear distortions. In our experiments, the BER is measured for all formats around the upper input power limit of the IPDR indicated by EVM_{lim}. At theses input powers, BER values of about $8 \cdot 10^{-10}$ for BPSK, $3 \cdot 10^{-9}$ for QPSK and $1.4 \cdot 10^{-3}$ for 16QAM are measured. Thus, the EVM is used to obtain a reliable tendency of the IPDR.

To study the IPDR limitations for low and high input power levels, the magnitude and phase errors (Fig. 11) relative to the BtB magnitude and phase values are evaluated. For low input powers it is seen from Fig. 11(a)-11(c) that magnitude and phase errors decrease with increasing input power. No difference can be seen between bulk and QD SOA. The behavior of the SOA samples differs, however, for large input powers. For BPSK and QPSK encoded signals the amplitude is virtually error-free, whereas the phase error significantly increases with increasing input power. For the 16QAM signal, both, magnitude and phase errors contribute to the EVM. In Section 2 the physical reasons leading to the measured results in Fig. 11 were discussed in detail.

We compare experimental results with the outcome of a numerical model, which was developed for a QD SOA. However, due to the admissible injection currents, we operate the QD SOA in a region were the wetting layer can be depleted to some extent [28] such leading to saturation effects and to a noticeable amplitude-phase coupling. The observable phase

#163313 - $15.00 USD Received 22 Feb 2012; revised 9 Apr 2012; accepted 9 Apr 2012; published 12 Apr 2012

recovery times are long enough so that numerically and experimentally there is no difference between QD and bulk SOA. What actually differs for physical devices, is the alpha factor, and this is reflected in the experimental and the numerical outcome.

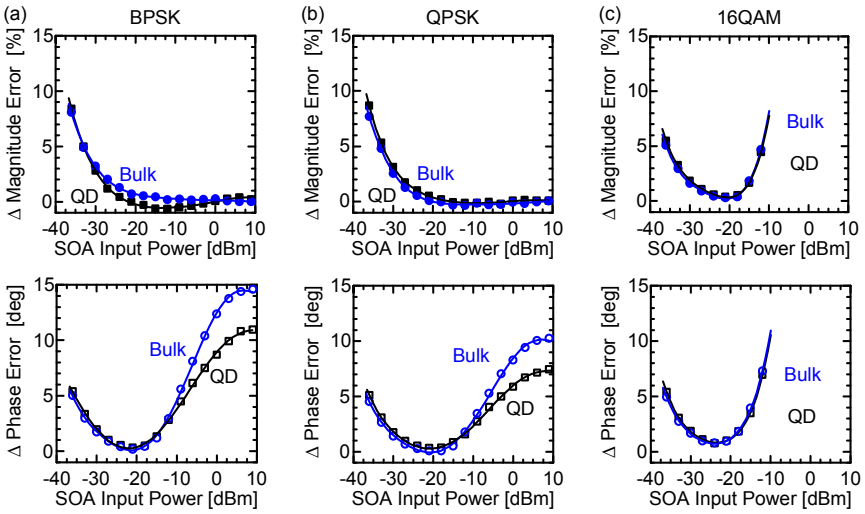

Fig. 11. Magnitude error and phase error increase as compared to BtB measurements. The degradation for low input powers is due to OSNR limitations. The upper limit is due to phase errors for (a) BPSK and (b) QPSK. Magnitude errors are insignificant. (c) At 16QAM the phase error is accompanied by gain saturation inducing magnitude errors. The alpha-factor impact decreases due to a lower probability for large power transitions.

In Table 3 the experimentally obtained results of the IPDR difference for both SOAs ($IPDR_{QDSOA} - IPDR_{bulkSOA}$) are compared to the simulation result for various modulation formats. The IPDR differences show good agreement between simulation and measurement within a range of 1 dB. While from the FREAG measurements Fig. 8 only the *ratio* of alpha factors for bulk and QD SOA could be extracted, the comparison of simulations with experiments now allows to conclude also the *absolute* values 4 and 2, respectively.

We checked that the symbol rate difference between simulation and measurement is of minor importance. Only for symbol rates larger than 35 GBd we found an increase of the upper IPDR limit P_2. The upper IPDR limit increases between 35 GBd (P_2 = 10 dBm) and 45 GBd (P_2 ~20 dBm) and it was tested with DPSK modulation and an alpha factor of 4.

Table 3. Comparison of measurement and simulation results for the difference of the IPDR for ithe lower alpha-factor SOA and the higher alpha-factor SOA for various modulation formats. The evaluation method, i. e. PP or EVM and the corresponding BER limit are defined according to Section 3. Measurements and simulations show the same tendency in spite of the fact that the symbol rate had to be reduced for the measurement from 28 GBd (as assumed for the simulations) to 20 GBd due to limitations in the available equipment. The pound character (#) indicates measured results for 28 GBd NRZ DQPSK taken from our previous work [16].

Format	$-\log_{10}$ BER	IPDR Difference	
		$IPDR_{QDSOA} - IPDR_{bulkSOA}$ [dB]	$IPDR_2 - IPDR_4$ [dB]
	(PP, EVM)	Measurement	Simulation
NRZ DQPSK	9 (PP)	5#[16]	4
NRZ BPSK	9 (EVM)	8	7
NRZ QPSK	9 (EVM)	4	5
NRZ 16QAM	3 (EVM)	0	1

#163313 - $15.00 USD Received 22 Feb 2012; revised 9 Apr 2012; accepted 9 Apr 2012; published 12 Apr 2012

5. Conclusion

Semiconductor optical amplifiers have been studied as amplifiers for advanced modulation formats. In particular we have studied the influence of the alpha factor on the amplification process. It is found that low alpha-factor SOAs are advantageous for purely phase encoded signals (BPSK, (D)QPSK). It is further found that an SOA with large alpha factor can be successfully used to amplify *M*-ary signals with a large number of amplitude levels. This is due to a lower probability for large power transitions in complex modulation formats which in turn reduces the influence of gain changes and the associated phase errors.

Acknowledgments

This work was supported by the Center of Functional Nanostructures (CFN) of the German Research Foundation (DFG), by the Karlsruhe School of Optics & Photonics (KSOP), by the European project EURO-FOS, by the Karlsruhe Nano-Micro Facility (KNMF), the BMBF project CONDOR, and the Agilent University Relations Program.

#163313 - $15.00 USD Received 22 Feb 2012; revised 9 Apr 2012; accepted 9 Apr 2012; published 12 Apr 2012